ELSEVIER

Contents lists available at ScienceDirect

Materials Science & Engineering A

journal homepage: www.elsevier.com/locate/msea



A comparative study of fatigue behaviour of MAG and laser welded components using reliability analysis



Marco Dourado ^{a,*}, Delfim Soares ^a, Joaquim Barbosa ^a, António Marques Pinho ^a, José Meireles ^a, Paula Branco ^b, Carlos Ribeiro ^c, Carlos Rei ^c

- ^a Mechanical Engineering Department, Azurém Campus, 4800-058 Guimarães, Portugal
- ^b Instituto de Soldadura e Qualidade, Rua do Mirante, no. 258, 4415-491 Grijó, VNG, Portugal
- ^c Sodecia Centro Tecnológico S.A, Rua Engenheiro Frederico Ulrich, 2650, 4470-605 Maia, Portugal

ARTICLE INFO

Article history:
Received 19 January 2014
Received in revised form
18 March 2014
Accepted 20 March 2014
Available online 27 March 2014

Keywords: Fatigue Reliability analysis Weld joint MIG/MAG Laser welding

ABSTRACT

Fatigue is one of the main causes of failure of structures and mechanical components, occurring due to the progressive weakening of their strength that reduces significantly their lifetime, when subjected to cyclic stresses over time. In welded components, the joints are the zones most susceptible to crack by fatigue.

Therefore, the base of this study are the Metal Inert Gas/Metal Active Gas (MIG/MAG) and LASER welding manufacturing processes, focused in three main areas involved in an automotive metallic system under dynamic loads: Fatigue testing in order to prevent structural collapse; Heat Affected Zones (HAZ) characterization to evaluate the material properties modification originated by those different technologies; Reliability analysis in order to analyse the performance of the samples and to select the best connection in terms of product life cycle. For this purpose, samples representative of industrial automotive applications (long welds) have been selected to carry out this work. Two types of connected specimens were manufactured, consisting of two steel plates of different thicknesses, overlapping and welded by the MAG process (type A) or the Laser process (type B). Metallographic characterization was performed for both typologies, namely macrostructural and microstructural characterization of the weld joint, and respective HAZ. Mechanical properties were inferred by measuring and mapping microhardness variation on the neighbour of the weld joint. Fatigue tests were carried out for specimens type A and type B, using 15 samples of each type that were tested under 3 levels of stress amplitude. The samples manufactured by the Laser process show better fatigue behaviour when compared to the samples manufactured by MAG welding. The better weld joint solution is proposed in accordance with the reliability analysis of the obtained fatigue test results.

© 2014 Elsevier B.V. All rights reserved.

1. Introduction

The industry, including automotive, struggles continuously with the need to increase competitiveness and profitability. Due to their structural importance, metallic components and systems represent the major part of the weight of an automobile. These metal components are connected together in order to create multiple subsets, to get the final product. Therefore, several sets of metallic components/systems need to connect together.

E-mail addresses: mdourado@dem.uminho.pt (M. Dourado), dsoares@dem.uminho.pt (D. Soares), kim@dem.uminho.pt (J. Barbosa), acmpinho@dem.uminho.pt (A. Marques Pinho), meireles@dem.uminho.pt (J. Meireles), pabranco@isq.pt (P. Branco), carlos.ribeiro@ct.sodecia.com (C. Ribeiro), carlos.rei@ct.sodecia.com (C. Rei). Due to specific structural needs, the dynamic requests change all over the metallic components/systems. In addition, the continuous search for lighter and more resistant solutions, with lower costs and reaching the dynamic specifications and quality, with a perfect repeatability of the manufacturing process, force the designers to continuously search for solutions in order to optimize this set of variables. Furthermore, if the metallic components/systems have to respect security's characteristics or are exposed to continuous environmental and mechanic attacks, they will require increased attention. Welding is the most used technological process to connect two components and MAG/MIG, TIG, Submerged Arc and Laser processes are those more commonly used in industrial applications.

It is known that the welded joint of two components is the most susceptible zone to initiate fatigue crack, reducing significantly the component lifetime [1].

Fatigue is the result of regular or irregular cyclic stresses imposed on the component, that may lead to fatigue cracks,

^{*} Corresponding author.

initially microscopic, that propagate to visible cracks, leading to the rupture of the component [2–4]. Residual tensile stresses along the welded joint imposed by heating and cooling cycles may cause a decrease of the fatigue life of welded components [5]. The weld joint geometry also has an important effect on the fatigue life of the structure. A defective weld geometry may also increase tensions in the welded joint [6–8]. Weld joint geometry depends on the process and the operation parameters, namely the welding energy, welding speed, voltage and electric current, and wire feed speed [9,10]. High welding speed decreases the arc exposure time and does not allow complete base material dilution. Consequently. penetration and the extension of the heat affected zone decrease. In the MAG process, the welding speed and energy are lower than those used on the Laser process. Thus, higher base material dilution, penetration and area of the heat affected zone can be expected [10-12]. However, concentration of residual stresses also increases [13,14]. The Laser process allows higher welding speed, thus shorter exposure time. However, the capacity to employ higher energy and at the same time low heat input, make the process very advantageous to be used in the construction of welded joints subject to fatigue [12].

Fatigue must be considered as a primary factor to take into account in the reliability of any structure or component. Reliability can be defined as the probability of a component or system to perform its function over a period of time, under certain conditions. Reliability engineering studies the components or systems lifetime through modelling and statistical analysis. With the probabilistic distribution of its useful life, it is possible to achieve the survival probability and to optimize the system performance [15]. Thus, it is natural that there is a great need to safely estimate the components and/or mechanical systems lifetime.

This article aims to compare the fatigue behaviour, and consequent reliability, of two components, now denominated by plates, joined by welding using two different technologies – MAG and Laser welding.

As stated above, the fatigue behaviour of the welded joint depends on the characteristics and parameters of the welding process that control the macro- and microstructures of the welded zone. On this study the microstructure of the two specimens is analysed. The macrostructure is analysed via Vickers microhardness and by measuring penetration and area of the heat affected zone. Through macrostructural and microstructural characterization, it is possible to infer the best mechanical behaviour of a specimen type in relation to another.

2. Experimental procedure

In this section it is explained the samples for experimental tests and the experimental procedures are described.

2.1. Starting samples

The specimen manufactured by MAG welding is denominated by type A, and the specimen manufactured by Laser welding is denominated by type B. Two welded sets of each type (A and B) were manufactured. The reliability analysis was applied to both specimens and is presented as a new approach when applied to the comparative study of the two weld typologies manufactured according to the above mentioned welding processes. The welded specimens consisted of two plates of different materials, DD13 and S355 MC, which chemical compositions are presented in Table 1. Plates DD13 and S355 MC were 2.5 and 3 mm thick, respectively.

Table 2 summarizes the characteristics of the 2 weld types. A long weld set (1300 mm) was selected in order to simulate the industrial welding practice, thus increasing the sensitivity of the reliability tests.

Table 1
Chemical composition (wt%) of the material used in welding (supplier data).

Constituents	EN10111 - DD13	EN10149-2 – S355MC
C	0.051	0.050
Mn	0.231	0.240
Si	0.010	0.019
P	0.015	0.012
S	0.011	0.009
Al	0.032	0.025
Nb	-	0
Ti	0.001	0
V	0.000	0
B	0.002	-
Cr	0.022	-

Table 2Types of specimens of welded joints.

Name of the specimen			Welding process
Type A	EN10149-2 – S355MC EN10111 – DD13	3 2.5	MAG
Туре В	EN10149-2 - S355MC EN10111 - DD13	3 2.5	Laser

2.2. Samples for fatigue analysis

Samples for fatigue analysis were obtained from two welded sets of each specimen (types A/MAG and B/Laser) with original dimensions $1300 \times 450 \times$ thickness (t) mm³, by sectioning them perpendicular to the weld joint, as shown in Fig. 1a. The sets are identified as "set A1" and "set A2" for specimen type A, and "set B1" and "set B2" for specimen type B.

One must bear in mind that unlike the scheme of the weld joint shown in Fig. 1a, the width of the MAG weld joint was not constant along the entire joint length, which did not happen in the joint obtained by the Laser process. Ten samples were cut from each welded set with dimensions shown in Fig. 1b, i.e. twenty samples of each specimen type (A and B).

2.3. Samples for metallographic analysis

Two samples for metallographic analysis, as shown in Fig. 1c, were collected from each welded set (A1, A2, B1 and B2), one from the central zone of the steel sheets and the other at 50 mm from the end, as shown in Fig. 1a. Total four samples were cut from each specimen type (A and B). The samples were cut perpendicular to the axis of the weld joint with an average width of 20 mm using a lubricated saw to prevent heating of the area to be analysed.

The samples surface were prepared for macrographic and micrographic analyses by traditional polishing techniques. The microstructure was enhanced by chemical attack with Nital 5 reagent.

2.4. Metallographic characterization

Each joint was characterized with respect to its geometry and dimensions through macrostructural analysis according to the following parameters: total area of the weld joint and HAZ of the base material. Microstructural analysis is made in order to evaluate the change in microstructure between the base material and the weld of each specimen. The samples for microstructural analysis are observed at an ampliation of 50×0 on an electronic

microscope. Furthermore an evaluation of the mechanical properties of the welded zone was performed by carrying out Vickers microhardness measurements, at room temperature, on a hardness testing machine, using 1000 g load and 30 s indentation time. 1000 g load was found to be a suitable value to obtain reliable hardness values, taking into account the constituents present in the weld joint and in the HAZ and their morphology. The distance between indentations was $\geq 1.5 \times \text{Lm}$, where Lm is the average size of the indentation. Two sets of indentations were made for each sample, along two different lines/directions: one on the longitudinal line of the weld joint, i.e., from the bottom plate and passing through the respective HAZ and a second along a line

perpendicular to the weld joint, from the lower plate to the upper plate, passing through the weld.

2.5. Fatigue testing

For each specimen type, are performed fatigue tests on 15 samples for 3 levels of stress amplitude σ_a , which was obtained 15 values of cycles of rupture N_r , i.e., 5 values of cycles of rupture N_r for each level of stress amplitude σ_a . The tests were performed at room temperature, on a servo-hydraulic fatigue testing machine, at a frequency of 10 Hz.

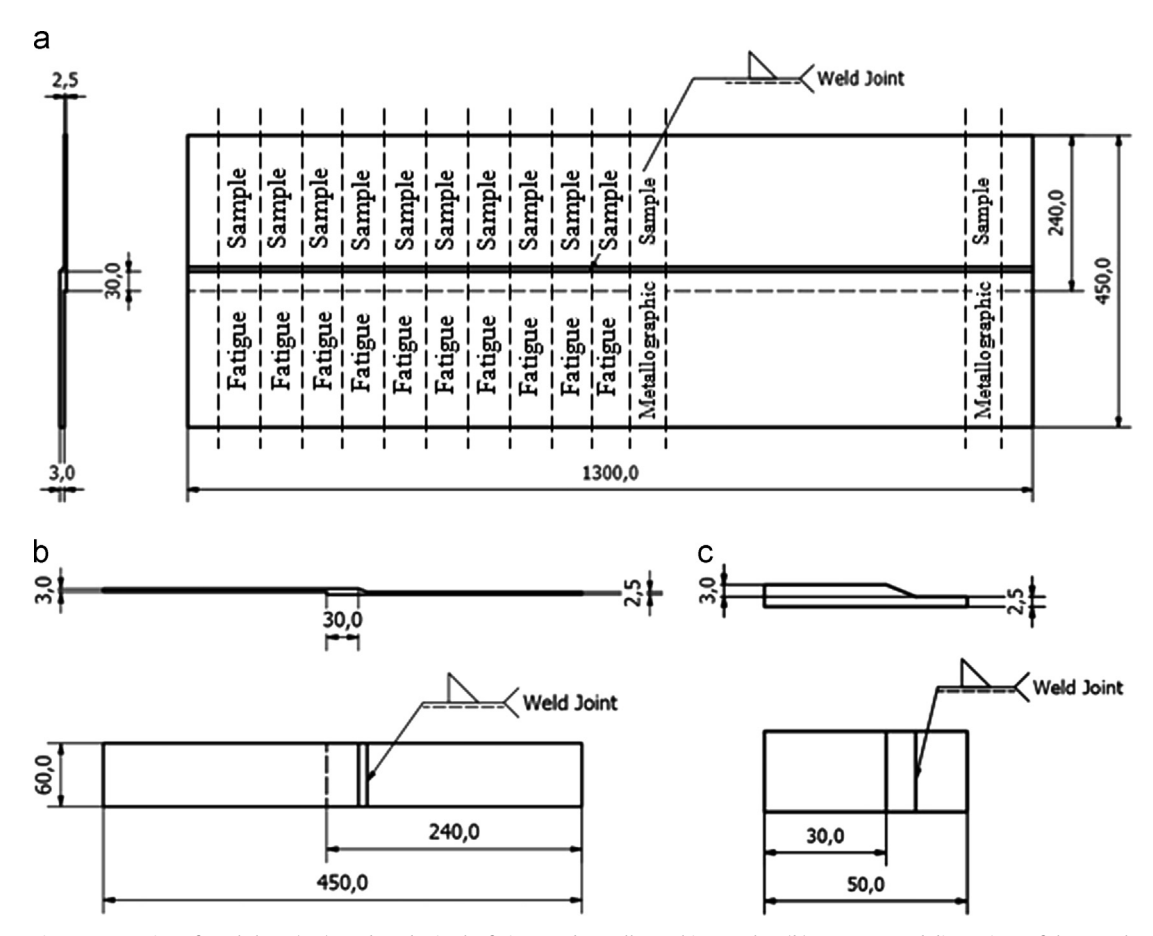


Fig. 1. (a) Schematic representation of steel sheet (set) used to obtain the fatigue and metallographic samples; (b) geometry and dimensions of the samples used for fatigue testing; (c) geometry and dimensions of the samples used for metallographic analysis.

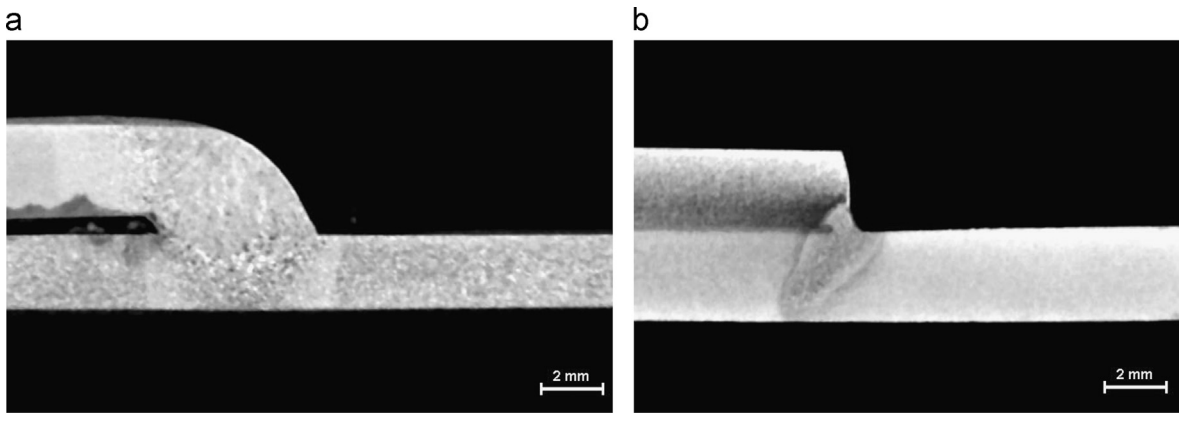


Fig. 2. Macrography representative of weld joints obtained with (a) MAG and (b) Laser welding processes.

3. Results and discussion

In this section the results and respective discussion are presented for all experimental tests and reliability analysis.

3.1. Macroscopic characterization and microhardness profiles of soldered samples

Results and discussion of macroscopic characterization and microhardness profiles of soldered samples are presented in this section for specimen types A and B.

3.1.1. Specimens of type A (MAG welding)

The macrographic analysis of the weld joints reveals, in general, excessive penetration and/or weld deposit in the bottom plate (lower thickness), as shown in Fig. 2.

The weld shape is regular and without faults along its entire length (1300 mm). No significant internal physical defects (cracks, porosities, etc.) have been detected. A displacement of the plates was observed in some cases (gap between plates in Fig. 2a) due to the high length of the samples and/or, probably, an inefficient positioning system.

Table 3Welded area quantification (weld zone and respective HAZ) of the MAG welded samples.

Samples	Area [n	Area [mm²]					
	Weld	DD13 HAZ	S355 MC HAZ				
Sheet centre metallographic sample of welded set A1	22.2	5.7	3.2				
Sheet end metallographic sample of welded set A1	12.5	3.0	0.9				
Sheet centre metallographic sample of welded set A2	12.4	3.1	4.0				
Sheet end metallographic sample of welded set A2	18.1	3.6	1.9				

Table 3 presents the quantification of areas of the weld zone and respective HAZ for the MAG welded samples, and Table 4 presents the average hardness quantification of the same samples. Fig. 3a is a schematic representation of the measured zones mentioned in Table 4.

The penetration of the bottom sheet steel of 2.5 mm is, in general, too high, leading to higher HAZ when compared with the 3 mm thick upper plate. This happens due to the differences on the plate thickness and suggests that current was too high for the 2.5 mm thick plate.

In general there is an increase on microhardness from the base materials to the respective HAZ and an even higher increase on the weld zone, with exception to Sheet Centre Metallographic Sample of Welded Set A1 and Sheet End Metallographic Sample of Welded Set A1, where microhardness on the HAZ zone is a little lower than on the S355 MC base material. Fig. 4 presents the hardness evolution along the weld zone for MAG weld type.

3.1.2. Specimens of type B (Laser welding)

The macrographic analysis of the Laser welded joints reveals, in general, a smaller weld area, as it can be seen in Fig. 2, when compared with MAG welded specimens. In general, Laser weld joints show full penetration in the bottom plate (thickness 3 mm) resulting of the position and orientation of the laser beam during the welding process. The HAZ is much lower than that obtained with MAG welding, as expected.

Table 5 presents the quantification of areas of the weld zone and respective HAZ of the Laser welded samples, and Table 6 shows the average hardness quantification of the same samples. Fig. 3b is a schematic representation of the measured zones mentioned in Table 6.

The small HAZ in DD13 material shows that the dilution area in this plate is very small for all samples welded by the Laser process.

In every welded sample, microhardness variation profiles reveal a significant increasing tendency from the base material to the centre of the weld. However, in the Laser welded samples there is a more significant and sudden increase when passing from the base material to the HAZ, and from the HAZ to the weld, which is justified by the low heat input with consequent increase of the

Table 4 Average microhardness quantification (base material, weld zone and respective HAZ) of the MAG welded samples.

Samples	Average microhardness [HV]							
	DD13 Material (Zone 1)	DD13 HAZ (Zone 2)	Weld (Zone 3)	S355 MC HAZ (Zone 4)	S355 MC Material (Zone 5)			
Sheet centre metallographic sample of welded set A1	123	130	200	147	155			
No. of measured points	4	6	2	2	2			
Sheet end metallographic sample of welded set A1	124	146	211	158	161			
No. of measured points	4	6	2	2	2			
Sheet centre metallographic sample of welded set A2	121	133	225	165	153			
No. of measured points	4	6	2	2	2			
Sheet end metallographic sample of welded set A2	126	140	196	164	153			
No. of measured points	4	6	2	2	2			

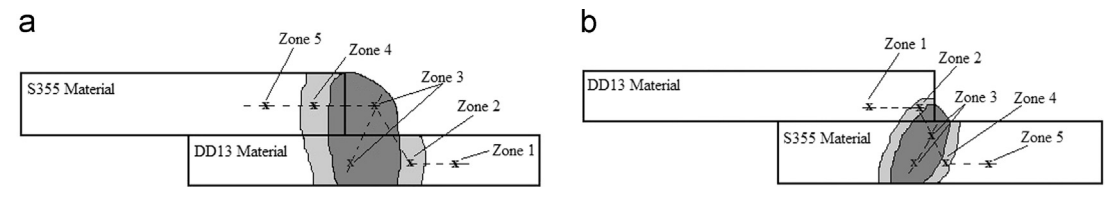


Fig. 3. Schematic representation of the measured zones for (a) MAG and (b) Laser welded samples.

cooling rate in the welding zone. Thus, with the Laser welding process, there is an average increase of 20% of microhardness in the weld zone in relation to the MAG welding process. Fig. 5 presents the hardness evolution along the weld zone for Laser weld type.

3.2. Microscopic characterization

The change in microstructure between the base material and the weld is less significant in the laser welded joints when

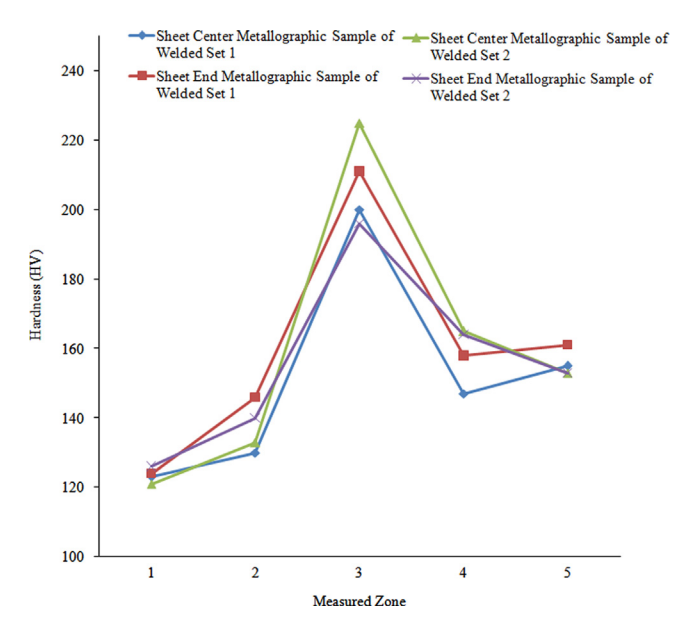


Fig. 4. Microhardness profile along the weld zone (longitudinal line) for MAG welding.

Table 5Welded area quantification (weld zone and respective HAZ) for the Laser welded samples.

Samples	Area [n	Area [mm²]				
	Weld	DD13 HAZ	S355 MC HAZ			
Sheet centre metallographic sample of welded set B1	3.2	0.7	1.3			
Sheet end metallographic sample of welded set B1	3.5	0.4	1.2			
Sheet centre metallographic sample of welded set B2	2.7	0.5	1.9			
Sheet end metallographic sample of welded set B2	4.9	0.4	3.4			

compared with those obtained by the MAG process, as shown in Fig. 6.

MAG welded samples present higher area of HAZ as well as higher grain size on that zone (Fig. 2a and Table 3). Physical defects, such as porosity and inclusions, were not differently detected on samples obtained by MAG or Laser welding.

3.3. Fatigue analysis

Results and discussion of fatigue analysis are presented in this section for specimen types A and B.

3.3.1. Specimens type A (MAG welding)

The number of fatigue cycles $N_{\rm r}$, presented in Table 7, shows good fatigue behaviour for the specimen type A, since the linear regression of S–N curve, shown in Fig. 7, is greater than 0.9, indicating quite low dispersion of results.

The samples break by the root weld severed, with the crack to spread along of the sheet steel. This fact results of a regular weld in terms of hardness, area and geometry.

3.3.2. Specimens type B (Laser welding)

The number of fatigue cycles N_r , presented in Table 8, shows good fatigue behaviour for the specimen type B, since the linear

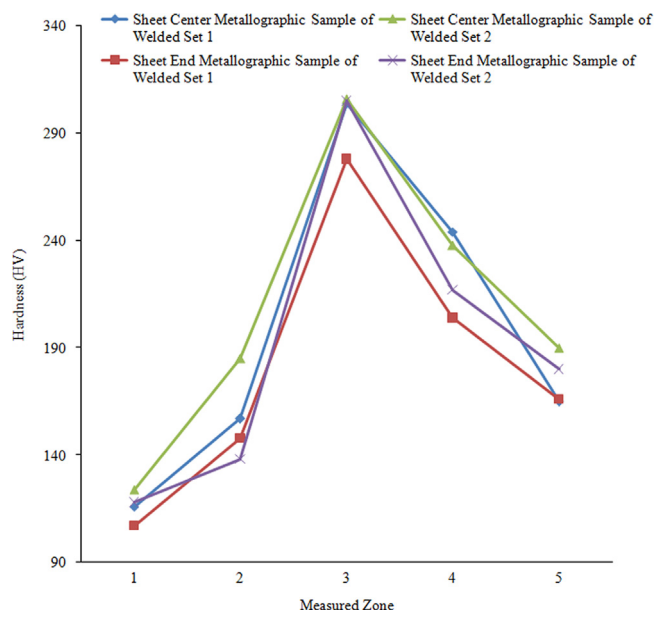


Fig. 5. Microhardness profile along the weld zone (longitudinal line) for Laser welding.

Table 6Average microhardness quantification (base material, weld zone and respective HAZ) for the Laser welded samples.

Samples	Average hardness [HV]							
	DD13 Material	DD13 HAZ	Weld	S355 MC HAZ	S355 MC Material			
	(Zone 1)	(Zone 2)	(Zone 3)	(Zone 4)	(Zone 5)			
Sheet centre metallographic sample of welded set B1	116	157	304	244	165			
No. of measured points	2	1	3	4	4			
Sheet end metallographic sample of welded set B1	107	148	278	204	166			
No. of measured points	2	1	3	4	4			
Sheet centre metallographic sample of welded set B2	124	185	306	238	190			
No. of measured points	2	1	3	4	4			
Sheet end metallographic sample of welded set B2	118	138	305	217	180			
No. of measured points	2	1	3	4	4			

regression of *S–N* curve, shown in Fig. 7, is greater than 0.9, indicating quite low dispersion of results.

The samples break by the root weld severed, with the crack spreading along the sheet steel. This fact results of n regular weld in terms of hardness, area and geometry.

Comparing these results with those obtained for the specimen type A, there is an increase in the average fatigue lifetime and less results dispersion, which is mainly due to the increased mechanical resistance in the weld performed by the laser welding process (see Tables 4 and 6). Although, the specimen type B have lower weld joint area. Due to the process characteristics, the concentration of residual stresses in the type B specimen is lower, which contributes to better fatigue behaviour of this specimen types.

With regards to the mechanical behaviour of materials and technologies, the large discussion is around the influence of the geometric irregularities of the weld joint, caused in each of these two technologies, MAG welding (Fig. 2a) and Laser welding (Fig. 2b). In this sense and in terms of the design of structures or mechanical components, their geometries directly influence the local stresses. Thus, in the case of welding type A it is evident that the geometric variation (irregularity) is more aggressive (more abrupt) and therefore the stress concentrations factor, Kt, is larger. Kt is defined as the ratio of the real stress, or effectively stress (highest stress), in the points of material that are under this effect, to the nominal stress (or reference stress). Thus, the effective local stresses (or real stress) are higher than

in case A compared to case B which will result in a lower fatigue life.

3.4. Reliability analysis results

In this section the reliability analysis results divided in parametric and non-parametric analysis results are presented. A comparative compilation summary of all reliability analysis results is also presented.

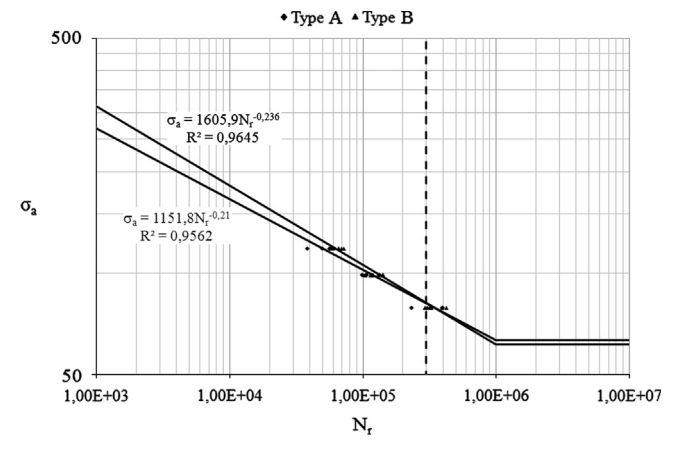


Fig. 7. S-N curves.

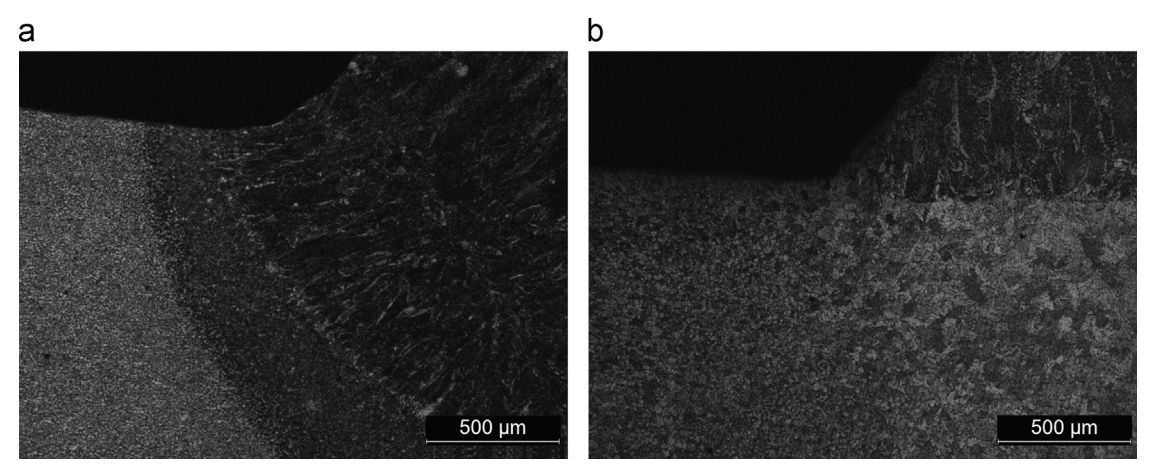


Fig. 6. Transition zone from weld to base material in joints obtained by the (a) Laser and (b) MAG welding processes.

Table 7Results of the fatigue tests for the samples of type A.

Sample reference	Minimum force [N]	Maximum force [N]	Stress amplitude $\sigma_{\rm a}$ [N/mm ²]	Frequency [Hz]	Test temp. [°C]	No. of cycles of rupture N_r [cycles]
Type A-1	185	18,483	119	10	22	56,134
Type A-2	180	18,003	119	10	22	57,152
Type A-3	180	18,099	119	10	22	49,904
Type A-4	181	18,084	119	10	22	61,608
Type A-5	181	18,126	119	10	22	38,343
Type A-6	152	15,180	99	10	22	133,097
Type A-7	151	15,065	99	10	22	106,859
Type A-8	155	15,456	99	10	22	116,751
Type A-9	152	15,242	99	10	22	99,546
Type A-10	152	15,183	99	10	22	131,279
Type A-11	121	12,068	79	10	22	397,570
Type A-12	117	11,740	79	10	22	394,315
Type A-13	123	12,269	79	10	22	325,001
Type A-14	120	12,002	79	10	22	320,861
Type A-15	121	12,078	79	10	22	233,291

3.4.1. Parametric analysis results

The reliability behaviour of the two samples is characterized using the parametric test used. Tables 9 and 10 summarize the results obtained for the specimen type A and the specimen type B, respectively.

3.4.2. Non-parametric analysis results

The Weibull distribution is the most widely used in studies of reliability, survival analysis and other areas due to its versatility.

The Weibull parameters were obtained by two different methods. One using linear regression and the other using Reliasoft software

Table 8Results of the fatigue tests for the samples of type B.

Sample reference	Minimum force [N]	Maximum force [N]	Stress amplitude $\sigma_{\rm a}$ [N/mm ²]	Frequency [Hz]	Test temp. [°C]	No. of cycles of rupture N_r [cycles]
Type B-1	179	17,934	119	10	22	72,299
Type B-2	180	17,949	119	10	22	58,631
Type B-3	177	17,672	119	10	22	66,219
Type B-4	184	18,394	119	10	22	69,015
Type B-5	180	18,020	119	10	22	65,757
Type B-6	152	15,148	99	10	22	142,449
Type B-7	151	15,123	99	10	22	142,526
Type B-8	151	15,117	99	10	22	103,666
Type B-9	151	15,075	99	10	22	118,690
Type B-10	150	15,040	99	10	22	114,789
Type B-11	119	11,930	79	10	22	423,397
Type B-12	120	11,956	79	10	22	392,505
Type B-13	120	12,016	79	10	22	293,760
Type B-14	121	12,046	79	10	22	303,898
Type B-15	121	12,112	79	10	22	325,926

Table 9 Parametric results for specimen type A.

Sample reference	Stress amplitude $\sigma_{\rm a}$ [N/mm ²]	Order no.	No. of cycles of rupture N_r [cycles]	Reliability $R(x)$	MTTF average failure [cycles]	Standard deviation [cycles]
Type A-5	119	1	38,343	0.8333	52,628	9012
Type A-3	119	2	49,904	0.6667		
Type A-1	119	3	56,134	0.5000		
Type A-2	119	4	57,152	0.3333		
Type A-4	119	5	61,608	0.1667		
Type A-9	99	1	99,546	0.8333	117,506	14,742
Type A-7	99	2	106,859	0.6667		
Type A-8	99	3	116,751	0.5000		
Type A-10	99	4	131,279	0.3333		
Type A-6	99	5	133,097	0.1667		
Type A-15	79	1	233,291	0.8333	334,208	67,221
Type A-14	79	2	320,861	0.6667		
Type A-13	79	3	325,001	0.5000		
Type A-12	79	4	394,315	0.3333		
Type A-11	79	5	397,570	0.1667		

Table 10 Parametric results for specimen type B.

Sample reference	Stress amplitude σ_a [N/mm ²]	Order no.	No. of cycles of rupture N_r [cycles]	Reliability $R(x)$	MTTF average failure [cycles]	Standard deviation [cycles]
Type B-2	119	1	58,631	0.8333	66,384	5061
Type B-5	119	2	65,757	0.6667		
Type B-3	119	3	66,219	0.5000		
Type B-4	119	4	69,015	0.3333		
Type B-1	119	5	72,299	0.1667		
Type B-8	99	1	103,666	0.8333	124,424	17,387
Type B-10	99	2	114,789	0.6667		
Type B-9	99	3	118,690	0.5000		
Type B-6	99	4	142,449	0.3333		
Type B-7	99	5	142,526	0.1667		
Type B-13	79	1	293,760	0.8333	347,897	57,095
Type B-14	79	2	303,898	0.6667		
Type B-15	79	3	325,926	0.5000		
Type B-12	79	4	392,505	0.3333		
Type B-11	79	5	423,397	0.1667		

Table 11 Non-parametric results for the specimen type A.

Sample reference	Stress amplitude $\sigma_{\rm a}$ [N/mm ²]	Order no.	No. of cycles of rupture N_r [cycles]	$F(x_i)$	β	η [Cycles]	MTTF average failure [cycles]	Standard deviation [cycles]
Type A-5	119	1	38,343	0.13	5.40	56,886	52,464	11,195
Type A-3	119	2	49,904	0.31				
Type A-1	119	3	56,134	0.50				
Type A-2	119	4	57,152	0.69				
Type A-4	119	5	61,608	0.87				
Type A-9	99	1	99,546	0.13	7.97	124,175	116,921	17,403
Type A-7	99	2	106,859	0.31				
Type A-8	99	3	116,751	0.50				
Type A-10	99	4	131,279	0.69				
Type A-6	99	5	133,097	0.87				
Type A-15	79	1	233,291	0.13	4.61	365,225	333,744	82,391
Type A-14	79	2	320,861	0.31				
Type A-13	79	3	325,001	0.50				
Type A-12	79	4	394,315	0.69				
Type A-11	79	5	397,570	0.87				

Table 12 Non-parametric results for the specimen type B.

Sample reference	Stress amplitude $\sigma_{\rm a}$ [N/mm 2]	Order no.	No. of cycles of rupture N_r [cycles]	$F(x_i)$	β	η [Cycles]	MTTF average failure [cycles]	Standard deviation [cycles]
Type B-2	119	1	58,631	0.13	13.01	68,771	66,097	6192
Type B-5	119	2	65,757	0.31				
Type B-3	119	3	66,219	0.50				
Type B-4	119	4	69,015	0.69				
Type B-1	119	5	72,299	0.87				
Type B-8	99	1	103,666	0.13	7.05	132,352	123,855	20,667
Type B-10	99	2	114,789	0.31				
Type B-9	99	3	118,690	0.50				
Type B-6	99	4	142,449	0.69				
Type B-7	99	5	142,526	0.87				
Type B-13	79	1	293,760	0.13	5.99	373,657	346,619	67,261
Type B-14	79	2	303,898	0.31				
Type B-15	79	3	325,926	0.50				
Type B-12	79	4	392,505	0.69				
Type B-11	79	5	423,397	0.87				

Table 13 Weibull results for the specimen type A and type B.

Name of the specimen	$\sigma_a = 119$ (N/mm ²)	σ_a =99 (N/mm ²)	σ_a =79 (N/mm ²)
Type A	β =5.41	β =7.99	β =4.61
	η =56,883 Cycles	η =124,170 Cycles	η =365,200 Cycles
	r=0.9671	r=0.9738	r=0.9612
Туре В	$\beta = 13.03$	β =7.06	β =6.00
	$\eta = 66,770$ Cycles	η =132,340 Cycles	η =373,620 Cycles
	r = 0.9772	r=0.9524	r=0.9302

Weilbull++7 package to confirm the values obtained numerically. Tables 11 and 12 summarize the results obtained for the specimen type A and specimen type B respectively, using the linear regression. Table 13 show the results obtained for the specimen type A and

specimen type B using Reliasoft software Weilbull + +7 package. Fig. 8 shows an example of a Weibull graphic of probability failure obtained for the specimen type B to the stress amplitude level

 σ_a =99 N/mm², using Reliasoft software Weilbull++7 package.

3.4.3. Reliability results summary

Table 14 presents a compilation of the results obtained by the different methods/tests referred above.

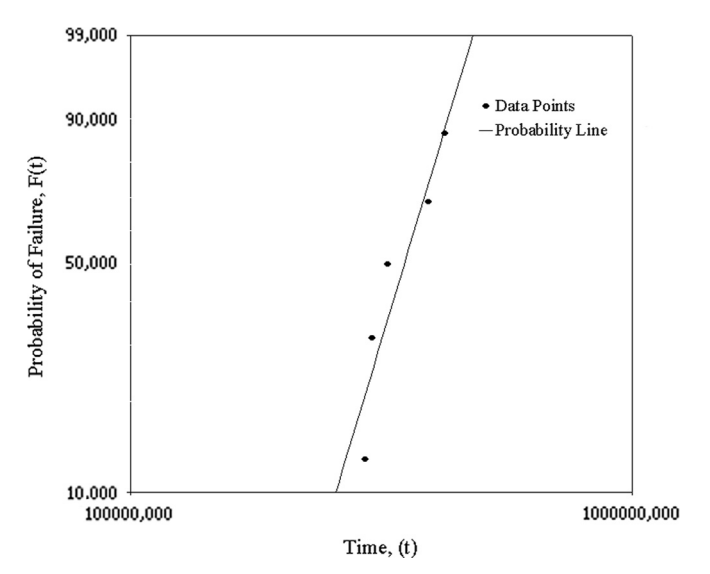


Fig. 8. Probability of failure vs. time Weibull graphic.

Based on the results obtained for the two types of specimens, it can be stated that the probability density function presents a welldefined peak and were best modelled with Weibull distribution.

Table 14Summary results for the tests that were carried out.

Type	Stress amplitude $\sigma_{\rm a}$ [N/mm ²]	Parameter	Parametric	Non-parametric numerical	Non-parametric software	Reliability expressions
A	119	MTTF [cycles] St. deviation [cycles] η [Cycles] β t_0	52,628 9012	52,464 11,195 56,886 5.4 63,415	56,883 5.41	$R(x) = e^{-(x - 63.415/56886)^{5.40}}$
	99	MTTF [cycles] St. deviation [cycles] η [Cycles] β t_0	117,506 14,742	116,921 17,403 124175 7.97 78,809	124,170 7.99	$R(x) = e^{-(x - 78.809/124175)^{7.97}}$
	79	MTTF [cycles] St. deviation [cycles] η [Cycles] β t_0	334,208 67,221	333,744 82,391 365225 4.61 352,206	365,200 4.61	$R(x) = e^{-(x - 325,206/365225)^{4.61}}$
В	119	MTTF [cycles] St. deviation [cycles] η [Cycles] β t_0	66,384 5061	66,097 6192 68,771 13.01 66,251	66,770 13.03	$R(x) = e^{-(x - 66.251/68771)^{13.01}}$
	99	MTTF [cycles] St. deviation [cycles] η [Cycles] β	124,424 17,387	123,855 20,667 132,352 7.05 120,797	132,340 7.06	$R(x) = e^{-(x - 120.797/132352)^{7.05}}$
	79	MTTF [cycles] St. deviation [cycles] η [Cycles] β t_0	347,897 57,095	346,619 67,261 373,657 5.99 285,116	373,720 6.00	$R(x) = e^{-(x - 285,116/373657)^{5.99}}$

The failure rate (MTTF $^{-1}$) increases with the magnitude of the number of operating cycles, representing the third phase of the bathtub curve, confirming the selection of the Weibull distribution, as a function of failure rate. This fact can also be confirmed with the values obtained for parameter β . For all stress ranges it was achieved values $\beta > 1$. These results were expected since the fatigue phenomenon is a cumulative process, having in consideration the nature of the mechanism of cracks initiation, propagation and, unimportant, final failure by fracture.

Both non-parametric and parametric test results are very similar which means that the distribution used to characterize the problem, fits the study needs.

Finally, according to the results obtained for MTTF, specimen type B is the one that presents better behaviour in terms of reliability. The MTTF values achieved for all stress ranges are higher for specimen type B, in other words, specimen type A will fail earlier in time than specimen type B.

4. Conclusions

The information obtained through this study, after being analysed in accordance with the reliability theory, allowed to graphically and analytically understanding the behaviour of the specimens tested in terms of failure rate and density probability function. With the laser welding technique a lower weld and HAZ area is, generally, obtained. The change in the microstructure, from metal base to the weld, is more smooth resulting in less residual stress concentration and expected improved mechanical properties. For this reason the fatigue behaviour is better for that joint configuration.

Acknowledgements

The authors gratefully acknowledge to the Centre for Mechanical and Materials Technologies (Centro de Tecnologias Mecânicas e de Materiais – CT2M) and COMPETE.

References

- [1] A. Ohta, N. Suzuki, Y. Maeda, Int. J. Fatigue 19 (1) (1997) 303-310.
- [2] D. Pilkey Walter, Peterson Stress Concentration Factors, 3rd edition, John Wiley & Sons, New York, 2009.
- [3] C.M. Moura Branco, A.A. Fernandes, P.T. Castro, Fadiga de estruturas soldadas, Fundação Calouste Gulbenkian, Lisboa, 1986.
- [4] M. Buciumeanu, A.S. Miranda, A.C.M. Pinho, F.S. Silva, Eng. Fail. Anal. 14 (2007)
- [5] N.T. Ninh, M.A. Wahab, J. Mater. Process. Technol. 48 (1995) 581–588.
- [6] X. Zhi-Gang, K. Yamada, Int. J. Fatigue 26 (2004) 1277–1293.
- [7] C.M. Sonsino, Int. J. Fatigue 31 (2009) 88-101.
- [8] C. Acevedo, A. Nussbaumer, Int. J. Fatigue 31 (2009) 88–101.
- [9] M.M. Alam, Z. Barsoum, P. Jonsén, A.F.H. Kaplan, H.A. Haggblad, Appl. Surf. Sci. 256 (2009) 1936–1945.
- [10] D.R. Alba, Influência dos parâmetros obre a geometria dos cordões produzidos por soldagem MAG robotizada, Universidade Federal do Rio Grande do Sul, Porto Alegre, 2013.
- [11] R.S. Polido, D.A. de Carvalho Junior, V.L. Júnior, M.R.V. de Araújo, J. Gallego, Caracterização da zona termicamente afectada em aço estrutural submetido à soldagem por arco submerso, UNESP, Faculdade de Engenharia de Ilha Solteira, Departamento de Engenharia. Mecânica. São Paulo. 2005.
- [12] S.-K. Cho, Y.-S. Yang, K.-J. Son, J.-Y. Kim, Finite Elem. Anal. Des. 40 (2004) 1059–1070.
- [13] A. Zeemann, Tensões residuais de soldagem, Infosolda, São Paulo, 2003.
- [14] B. Weiss, G.E. Grotke, R. Stickler, Weld. Res. Suppl. 49 (1970) 471–487.
- [15] M.J. Simonetti, A.L. Souza, L.F.S. Silveira, J.P.S. Arruda, A importância da engenharia da confiabilidade e os conceitos básicos de distribuição de Weibull.